A Sampling Strategy for Remotely Sensed LAI Product Validation Over Heterogeneous Land Surfaces

Yelu Zeng, Jing Li, Qinhuo Liu, Longhui Li, Baodong Xu, Gaofei Yin, and Jingjing Peng

***Abstract*—The development of efficient and systematic ground-based spatial sampling strategies is critical for the validation of medium-resolution satellite-derived leaf area index (LAI) products, particularly over heterogeneous land surfaces. In this paper, a new sampling strategy based on high-resolution vegetation index prior knowledge (SSVIP) is proposed to generate accurate LAI reference maps over heterogeneous areas. To capture the variability across a site, the SSVIP is designed to 1) stratify the nonhomogeneous area into zones with minimum within-class variance; 2) assign the number of samples to each zone using Neyman optimal allocation; and 3) determine the spatial distribution of samples with a nearest neighbor index. The efficiency of the proposed method was examined using different vegetation types and pixel heterogeneities. The results indicate that the SSVIP approach can properly divide a heterogeneous area into different vegetation cover zones. Whereas the LAI reference maps generated by SSVIP attain the target accuracy of 0.1 LAI units in cropland and broadleaf forest sites, the current sampling strategy based on vegetation type has a root mean square error (RMSE) of 0.14 for the same number of samples. SSVIP was compared with the current sampling strategy at 24 VALERI sites, and the results suggested that samples selected by SSVIP were more representative in the feature space and geographical space, which further indicated the reasonable validation over heterogeneous land surfaces.**

***Index Terms*—Heterogeneous pixel, leaf area index (LAI), prior knowledge, product validation, sampling strategy.**

I. Introduction

THE LEAF AREA index (LAI) is a key parameter for ecosystem process models [1]–[3]. Satellite remote sensing provides a unique way to obtain the LAI at regional to global scales. In recent years, several global LAI products have been derived from sensors, such as TERRA&AQUA/MODIS [4], SPOT/VEGETATION [5], ENVISAT/MERIS [6], TERRA/MISR [7], and AVHRR [8], [9]. Validation and accuracy assessment of these LAI products are important for product utilization, algorithm improvement, and product refinement [10].

Many ground observation programs at the global or continental scale have been implemented, such as the BOREAS and Bigfoot programs in North America [11]–[13], SAFARI2000 in Africa [14], VALERI in Europe, and WATER in China [15]. The early observation programs were mainly validated over relatively homogeneous landscapes, and the arithmetic mean of several *in situ* measurements was typically regarded as the true value of a pixel [16], [17]. However, the validation of medium-resolution products over heterogeneous land surfaces is challenging because ground-based measurements are typically spatially limited, and direct comparison of the products may not be reasonable due to spatial heterogeneity [18]. A generally accepted "bottom-up" validation approach based on a two-stage sampling strategy can solve the problem of scale-mismatch between ground point measurements and the pixels [19], [20]. This approach employs both field measurements and high-resolution satellite data to establish a site-specific relationship (transfer function) and to generate high-resolution LAI reference maps over the site. The LAI reference maps are then aggregated to a 1-km resolution and used as benchmarks to validate the products [21]. This framework can be adapted to validations over nonhomogeneous land surfaces. However, the accuracy of this methodology depends largely on the precision of the field measurements, imperfect atmospheric corrections, calibration and geolocation errors of the high-resolution satellite data, sampling strategy, and land surface heterogeneity [10], [21]. The spatial sampling strategy is a key step in the validation process of generating LAI reference maps. Different sampling strategies will generate different coefficients of the transfer function and ultimately affect the accuracy assessment of the LAI product.

The three most commonly used sampling strategies are random, systematic and stratified sampling [22]. The simplest sampling strategy is random sampling, in which the sample locations are selected by a series of random numbers [17], [23], [24]. In the random sampling strategy, each unit in the site has an equal and independent chance of selection. However, the sampling variance is typically larger than other methods for the same number of samples because large empty spaces and aggregation of sampling points may occur. The systematic sampling strategy generates a regular grid to determine the sample locations. The grid can be square, rectangular, hexagonal, or any other shape [14], [16], [25], [26]. Samples selected by this method are uniformly spread across the geographic space, but each unit in the site does not have an equal probability of selection, and minor class types may have rare sample units and be under-represented. The two strategies described above are

Manuscript received September 16, 2013; revised March 03, 2014; accepted March 08, 2014. Date of publication April 03, 2014; date of current version August 21, 2014. This work was supported in part by the National Natural Science Foundation of China (41271366), in part by the National Basic Research Program of China (2013CB733401), and in part by the National High Technology Research and Development Program of China (2012AA12A304 and 2012AA12A305). *(Corresponding authors: J. Li and Q. Liu.)*

Y. Zeng, J. Li, Q. Liu, B. Xu, G. Yin, and J. Peng are with State Key Laboratory of Remote Sensing Science, Institute of Remote Sensing and Digital Earth, Chinese Academy of Sciences, Beijing Normal University, Beijing 100101, China (e-mail: lijing@irsa.ac.cn; qhliu@irsa.ac.cn).

L. Li is with Plant Functional Biology and Climate Change Cluster (C3), University of Technology, Sydney 2007, Australia.

Y. Zeng, B. Xu, G. Yin, and J. Peng are also with the College of Resources and Environment, University of Chinese Academy of Sciences, Beijing 100049, China.

Color versions of one or more of the figures in this paper are available online at http://ieeexplore.ieee.org.

Digital Object Identifier 10.1109/JSTARS.2014.2312231

based on the assumption that there is no prior knowledge about the sampling site, and both methods are able to achieve satisfactory accuracy in relatively homogeneous areas. However, the land surface is typically heterogeneous at moderate or coarse resolution, and thus, both methods may not guarantee an accurate validation. Stratified sampling has the potential to use *a priori* knowledge, such as vegetation types, to partition the area into relatively homogeneous subareas (zones) and therefore capture the heterogeneity of the land surface. Recent research has attempted to employ readily available prior knowledge, such as land cover types or soil types, to design a more efficient sampling strategy and to achieve the same accuracy with fewer samples [27]–[29]. This method is potentially the most efficient approach and is widely used in current field campaigns, such as the VALERI project, Maun in Botswana, the Harvard Forest in the USA, and the Ruokolahti Forest in Finland [30]–[32].

Determining the true LAI value of the land surface is crucial in LAI product validation. The optical (chlorophyll, leaf water content) and structural (leaf angle distribution) properties of leaves and soil reflectance are important parameters in radiative transfer modeling and LAI retrieval algorithms [33], [34]; however, these parameters do not impact the true LAI value of a validation site. The method used to build the transfer function determines the choice of the prior knowledge [32], [35]. A uniform empirical relationship between the LAI and the reflectance or vegetation index (VI) is widely used to build the transfer function [10], [18]. This approach assumes that the LAI is the primary influence on the reflectance or VI for a given vegetation type and that the impact of variations of the leaf optical and structural properties and soil reflectance on the transfer function is limited when applied at the local scale of a validation site. Samples that can represent the feature and spatial distribution characteristics of the sampling area are crucial to ensure the accuracy of the transfer function. In ground sampling schemes for LAI validation, such as in the VALERI project, a vegetation classification map is commonly used, and the number of samples for each type is allocated in proportion to the areas of the vegetation types across the entire site [30], [32]. However, prior knowledge provided by the classification map is limited when there is a single vegetation type but the vegetation density varies, such as in grassland and forest [36]. The VI, the variability of which represents the heterogeneity of the vegetation's growth conditions, is more suitable as *a priori* knowledge. Although the VI is a compound effect of the leaf optical properties, leaf structural properties, and soil reflectance, it has a strong relationship with the LAI and is generally accepted to be a representative indicator of the LAI. However, the VI is not employed in the existing LAI sampling strategies.

The aim of this study was to propose a sampling strategy based on VI prior knowledge (SSVIP) that is more suitable for LAI validation over heterogeneous land surfaces than existing strategies. Section II describes why the VI map is appropriate for optimizing the sampling strategy of *in situ* LAI measurements from sampling theory and then proposes the SSVIP method. Section III designs a direct sampling efficiency evaluation procedure based on a PROSAIL model simulation [33] and using the bottom-up framework. Section IV compares the SSVIP method with the current sampling strategy based on vegetation type and analyzes the sampling accuracy and stability, sample number and heterogeneity, representative elementary sampling unit (ESU) in the feature and geographical space, and LAI reference map accuracy. In Section V, SSVIP is compared to the existing sampling strategy at 24 VALERI sites by comparing the normalized difference VI (NDVI) cumulative frequency distributions of the population with those of the ESUs using several sampling strategies. Section VI summarizes the SSVIP method, analyzes the deficiencies of SSVIP, and discusses future research directions.

II. Methodology

A. Theoretical Analysis

In LAI product validation, the goal of proposing an efficient sampling strategy is to improve the accuracy of the LAI reference map. In this section, we analyze how the efficiency of the sampling strategy could be improved by using the VI as *a priori* knowledge.

Assume that the validation site consists of m medium-resolution pixels and that each medium-resolution pixel contains k high-resolution pixels. Therefore, the validation site consists of mk high-resolution pixels (the population). In general, the site-specific relationship (transfer function) between the field measured LAI of each ESU and the single VI (SVI), such as NDVI and simple ratio (SR), is a univariate exponential or linear regression. The transfer function is applied to the entire site to generate the high-resolution LAI reference map, and the LAI reference map is then aggregated to medium resolution to validate the remotely sensed LAI product. By the independent residual assumption, the mean prediction error between the aggregated LAI reference map and the true value is [35]

$$\bar{\sigma}^2 = \frac{1}{k} MSE \left[1 + \frac{1}{n} + \frac{\sum_{t=1}^{mk} (x_t - x^{-})^2}{mk \sum_{i=1}^{n} (x_i - x^{-})^2} \right] = \frac{1}{k} MSE \left[1 + \frac{1}{n} + \frac{S_X^2 + (\bar{X} - \bar{x})^2}{n \cdot s_x^2} \right] \quad (1)$$

where x is the VI value of the high-resolution pixel, n is the number of samples, MSE is the mean square error between the true value and prediction value of the samples, $\bar{x}$ and s_x are the mean and standard deviation of the high-resolution VI value of the samples, respectively, and $\bar{X}$ and S_X are the mean and standard deviation of the high-resolution VI value of the entire site, respectively. Equation (1) illustrates that for a given dataset, when $MSE, n, m, \bar{X}$, and S_X are fixed, the mean prediction error is affected by the difference between the sample and population means ($\bar{X} - \bar{x} \to 0$) and the sample variance ($s_x \to \max$). In other words, the samples should be unbiased and be spread across the feature space. An appropriate sampling strategy should sample regularly along the feature space and proportionally represent it. Such sampling can be achieved by stratifying the entire validation site proportionally to the histogram of LAI or the reflectance data such that the samples and entire site have

similar histograms, and thus, the samples will be unbiased and have good coverage across the feature space. Thus, stratifying based on the VI is a more direct way to improve the sampling efficiency compared with stratifying based on vegetation types.

B. Sampling Strategy Based on VI Prior Knowledge (SSVIP)

According to the theoretical analysis presented above, an optimal sampling strategy must satisfy the following two requirements.

1) The samples should be unbiased to guarantee that there are no differences between the sample and population mean ($\bar{X} - \bar{x} \to 0$).
2) The samples should be spread across the feature space to maximize the sample variance ($s_x \to \max$).

However, these two points based on the theoretical analysis are not sufficient. If there is no penalty on spatial clustering, optimization only in the feature space may lead to spatial clustering of the sample locations. In a multiple linear regression function, the residuals are assumed to be independent. However, in practice, the residuals will often be spatially auto-correlated, and thus, the estimation of the regression coefficients is overly optimistic [37]. To minimize the effect of the spatially dependent characteristics of the residuals, the sample locations should have a maximum geographical spread [35]. Cochran [38] also noted that to estimate the spatial means of an environmental variable, the accuracy of the result will typically increase by dispersing the sample locations for better coverage of the study area. Therefore, an optimal sampling strategy has one additional requirement:

1) The samples should be spread across the geographical space.

To satisfy the above requirements, five steps are generally needed to implement SSVIP as follows.

Step 1) *Deriving an appropriate high-resolution VI map*

The high-resolution VI map is used as *a priori* knowledge to determine the distribution and number of samples. First, the acquisition date of the high-resolution imagery should be close to the sampling date to guarantee that the spatially heterogeneous characteristics have not changed. Second, special attention should be paid to the radiance calibration and geometric correction of the imagery to guarantee accurate top-of-atmosphere (TOA) and top-of-canopy (TOC) reflectance. Atmospheric correction is not mandatory if it is safe to assume that the effect of the atmosphere is the same over the entire site [19]. Finally, an appropriate VI whose variations are sensitive to vegetation density must be selected. The NDVI may be a good choice at low LAI values; however, the NDVI easily reaches saturation during the summer in some dense forest sites, which prevents this index from identifying changes in the LAI [39]. The SR or RSR may be alternative choices if the NDVI becomes saturated at high LAI values.

Step 2) *Setting the number of samples*

The number of ESUs depends on the extent of the validation site, its variability, and the size of the ESUs [19]. This number is also constrained by the manpower resources and time. At present, there is no quantitative method to determine the sampling number for a specific area. Baret *et al.* [32] recommended that 30–50 ESUs (20×20 m^2) were appropriate for a 3×3 km^2 site. In general, the number of ESU should be increased for a more heterogeneous surface or a larger study site.

Step 3) *Setting the optimal segmentation threshold*

For stratified sampling, when the number of allocated sample points within each stratum (n_h) is fixed, the expected sampling variance depends on the weighted sum of the variances within the strata. The lower within-class variance σ_h^2 results in a lower expected sampling variance. Therefore, we set the weighted sum of the variances within the strata as the objective function (*OF*)

$$OF(L,T) = \sum_{h=1}^{L} W_h \sigma_h^2 \tag{2}$$

where W_h is the corresponding weight assigned to the hth stratum, $W_h = N_h/N$, where N_h is the number of populations within the hth stratum, and N is the number of populations in the entire site. L is the stratum number, which ranges from one to N and is an integer. In general, larger values of L will result in smaller OF values. The optimal segmentation threshold (T) is calculated by minimizing the OF.

In Section III, L is assigned to be equal to the number of vegetation types to compare SSVIP with the current sampling strategy, which is based on vegetation type. We use the vegetation type map according to the non-supervised k_means classification method implemented in the VALERI campaign reports and the detailed vegetation status description of each ESU. In general, SSVIP will perform better with more vegetation density levels because it will lead to a smaller OF in (2). Thus, in Section V, the stratum number (L) is set to be equal to the number of samples to achieve the highest efficiency.

Step 4) *Assigning the number of samples to each stratum*

Because the population variance of each stratum σ_h^2 is known, we can use Neyman optimal allocation to assign the number of samples of each zone to have the lowest sample variance. For a fixed sample number n,

$$\frac{n_h}{n} = \frac{W_h \sigma_h^2}{\sum_{h=1}^{L} W_h \sigma_h^2} = \frac{N_h \sigma_h^2}{\sum_{h=1}^{L} N_h \sigma_h^2} \tag{3}$$

where n_h is the number of samples within the hth stratum. The weight of each sample in the hth stratum is W_h/n_h. The intuitive meaning of Neyman optimal allocation is that more sampling points should be assigned to a stratum if it has a larger area and a more significant variation than other strata.

Step 5) *Determining the spatial distribution of each sample point*

Steps 1–3 considered the feature space of the study site to assign the samples to the strata. The structure of the geographic space must be considered when assigning samples to each stratum. The samples should be

dispersed to assure a better spatial representation of the site. The nearest neighbor index (NNI), which is one of the most widely used distance statistics, is recommended to be used to describe the point distribution pattern [40]. The nearest neighbor distance $d(NN)$ is calculated as follows:

$$d(NN) = \sum_{i=1}^{n} \frac{\min(d_{ij})}{n} \tag{4}$$

where $\min(d_{ij})$ is the distance between each point and the point nearest to it and n is the number of sampling points. The mean random distance $d(ran)$ is then calculated, which is the $d(NN)$ value that one would expect if the distribution were random

$$d(ran) = 0.5\sqrt{A/n} \tag{5}$$

where A is the area of the site and n is the number of sampling points. Finally, the NNI is computed as follows:

$$NNI = \frac{d(NN)}{d(ran)}. \tag{6}$$

The ratio is equal to one when the distribution is random. Values less than one indicate aggregation, whereas values greater than one indicate a dispersed distribution. In the sampling area, 1000 groups of sampling points are randomly generated for a fixed number of samples in each stratum. The group combination that has the highest NNI value is selected as the optimum sample set.

III. Efficiency Evaluation Procedure

Evaluating the efficiency of a sampling strategy directly is challenging because the true values of the population are typically unavailable in practice, which is why sampling is necessary. In this study, we design a direct sampling efficiency evaluation procedure based on a PROSAIL model in the framework of a "bottom-up" LAI product validation procedure [19]. The procedure is shown in Fig. 1.

In the proposed evaluation procedure, the high-resolution LAI map and vegetation classification map are required before sampling to drive the PROSAIL model to simulate the high-resolution reflectance imagery. The general medium-resolution LAI product validation workflow was then conducted using different sampling strategies. The different sampling strategies resulted in different transfer functions, and thus, different LAI reference maps were generated. Finally, the LAI reference maps were aggregated to medium resolution. The high-resolution LAI map was regarded as the true value LAI dataset; it was aggregated to medium resolution and served as a benchmark for evaluating the LAI reference maps. The efficiency of the different sampling strategies can thus be analyzed and evaluated.

Two areas covered by crop and broadleaf forest (Fig. 2) were used to evaluate the efficiency and analyze the sampling strategy. The two sites correspond to agricultural fields and natural forest, which have different spatial structures and variability characteristics. The cropland site is in Sud-Ouest, France, and covers an

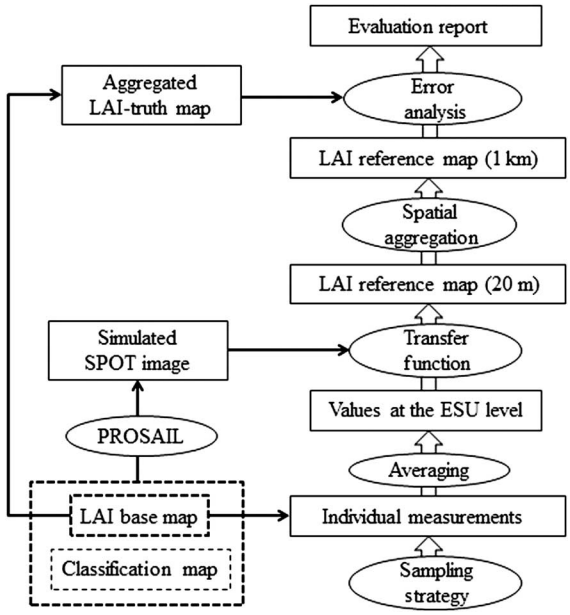

Fig. 1. Sampling efficiency evaluation framework based on the PROSAIL model.

area of 3×3 km^2. It includes five classes. Class 1 is composed of soy beans and woodland, Class 2 is composed of poplars, fallow fields, and grassland, Classes 3 and 4 are composed of mature or harvested wheat fields and fallow fields, and Class 5 is composed of corn, soy beans, and sunflowers [41]. The broadleaf forest area is located in Camerons, Australia, and covers an area of 4×4 km^2. It corresponds to a natural Australian forest on gently undulated topography. The vegetation is composed of several local species, and the understory is relatively dry with sparsely distributed grasses and bushes. This site consists of four classes. Class 1 is composed of tea trees, Class 2 is composed of casuarina, Class 3 is composed of banksia and blackbutt, and Class 4 includes wide forest roads [42].

The simulation of high-resolution reflectance imagery, ESU sampling strategy, simulated individual measurement, and transfer function are introduced below.

A. Simulation of High-Resolution Reflectance Imagery

The objective of the simulation is not to obtain the real satellite image but to determine the true LAI values and vegetation canopy reflectance simultaneously for the analysis and evaluation. The PROSAIL model was used to simulate the high-resolution reflectance map. The 20-m-resolution LAI map provided by the VALERI dataset was used as the input parameters to drive the PROSAIL model. Due to the lack of information on the leaf biochemical properties of each vegetation type and the soil reflectance at the study sites, we used reasonable values of typical vegetation types provided by the vegetation status description of each ESU provided by the VALERI campaign reports [41], [42] as input parameters to simulate the images of the two sites. A typical soil spectrum from the spectral library [43] was used in the PROSAIL model, which includes reflectances of 0.195 and 0.297 in the red and near-infrared (NIR) bands, respectively. Tables I and II provide the value of each input parameter of each vegetation type [33]. N is the leaf structure parameter that

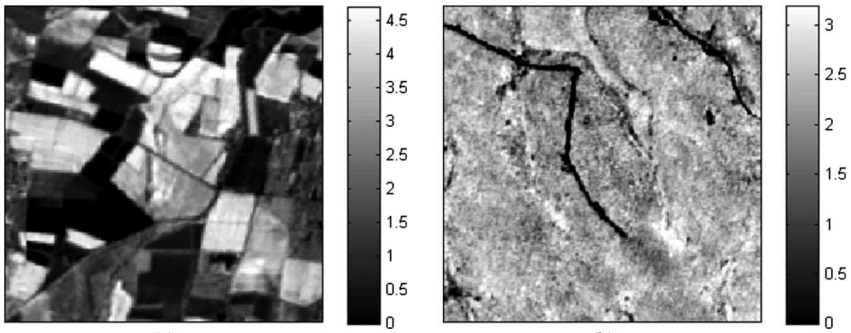

Fig. 2. 20-m resolution LAI maps of (a) the Sud-Ouest site and (b) the Camerons site. The Sud-Ouest site covers an area of $3\ \mathrm{km} \times 3\ \mathrm{km}$, and the dominant vegetation type is cropland. The Camerons site covers an area of $4\ \mathrm{km} \times 4\ \mathrm{km}$, and the dominant vegetation type is broadleaf forest.

TABLE I
VALUES OF THE INPUT PARAMETERS TO DRIVE PROSAIL SIMULATION FOR FIVE CLASSES AT THE SUD-OUEST SITE

Class type	N	C_{ab} (μg/cm^2)	C_w (cm)	C_m (g/cm^2)	ALA (°)
Woodland	1.826	47.7	0.0003	0.0043	26.76
Grassland	1.875	46.7	0.0100	0.0030	45
Harvested wheat fields(a)	2.275	23.7	0.0075	0.0058	63.24
Harvested wheat fields(b)	2.275	23.7	0.0075	0.0058	63.24
Corn	1.518	58.0	0.0131	0.0037	57.3

TABLE II
VALUES OF THE INPUT PARAMETERS TO DRIVE PROSAIL SIMULATION FOR THREE CLASSES AT THE CAMERONS SITE

Class type	N	C_{ab} (μg/cm^2)	C_w (cm)	C_m (g/cm^2)	ALA (°)
Tea trees	2.660	74.1	0.0199	0.0135	26.76
Casuarina	2.656	62.8	0.0003	0.0066	26.76
Banksia and blackbutt	1.826	47.7	0.0003	0.0043	26.76

denotes the number of homogeneous layers, C_{ab} is the chlorophyll a and b content, C_w is the equivalent water thickness, and C_m is the dry matter content. ALA is the average leaf inclination angle. The leaf inclination angle distribution patterns of the vegetation types at Sud-Ouest, including woodland, grassland, wheat, and corn, are set as planophile, uniform, plagiophyre, and spherical, respectively [44]. The leaf inclination angle distribution at Camerons is set as planophile for the broadleaf canopy cover.

For the image simulation, C_{ab} and C_m are assigned to change by $\pm 10\%$. The view illumination geometries are set according to the SPOT data from which the high-resolution LAI map was derived [41], [42]. Because N and ALA are closely related to the vegetation type, the input values are held constant for one class. The C_w value is also held constant for pixels of one class because the simulated bands are not in the water absorption bands. The spectral response function of SPOT4 was used to simulate the band spectra.

Considering the errors caused by such factors as the imperfect atmospheric correction and geolocation uncertainties, Gaussian noise was added to the reflectance imagery. The theoretical estimation of the relative uncertainties for the atmospherically corrected MODIS green, red, and NIR spectral bands are $\sigma_{\mathrm{green}} = 0.1$, $\sigma_{\mathrm{red}} = 0.2$, and $\sigma_{\mathrm{NIR}} = 0.05$, respectively [45]. We added corresponding Gaussian white noise to the reflectance imagery.

TABLE III
TRANSFER FUNCTIONS AND THE CORRESPONDING RMSE AND R^2 OF TWO METHODS AT THE TWO STUDY SITES

		Transfer function	RMSE	R^2
Sud_Ouest	Method 1	$0.20 \times SR - 0.02$	0.54	0.86
	Method 2	$0.20 \times SR + 0.03$	0.52	0.89
Camerons	Method 1	$0.16 \times SR - 0.07$	0.60	0.81
	Method 2	$0.12 \times SR + 0.40$	0.56	0.83

B. ESU Sampling Strategy

Because Martinez *et al.* [31] confirmed that the recently used stratified sampling strategy performs better than systematic sampling, we compared SSVIP (Method 1) to the current sampling strategy based on vegetation types (Method 2), which allocated the number of samples in proportion to the areas covered by the vegetation types across the entire site.

The generation of sampling points by SSVIP follows the process described in Section II-B. The corresponding NDVI and SR maps are derived using the simulated high-resolution reflectance imagery. The NDVI was a good choice at Sud-Ouest. At Camerons, NDVI reaches saturation, so the SR was used instead. To compare with the sampling based on vegetation types, the VI map is classified with the same number of classes as the number of vegetation types. The optimal segmentation thresholds are determined by the OF in (2); the intervals are [0, 0.33), [0.33, 0.52), [0.52, 0.71), [0.71, 0.85), and [0.85, 1) for NDVI at Sud-Ouest and [0, 6.85), [6.85, 12.00), [12.00, 14.97), and [14.97, 23.53) for SR at Camerons. In the analysis, the number of samples ranges from 10 to 100 with a step of 10, and the number of samples assigned to each class is consistent with Neyman optimal allocation. The optimum sample set is selected by NNI as discussed in Section II-B.

C. Simulated Individual Measurement

Field measurements always differ from the true values because of measurement errors. Field measurement errors are caused by optical instrument calibration, saturation of the optical signal in dense canopies, insufficient spatial sampling within the ESU, and geolocation errors [46], [47]. In the validation procedure based on the model simulation, we add 20% Gaussian white noise to the LAI map and then set the corresponding value as the individual measurement. Considering the noise in the data, this step was repeated $N = 1000$ times to test the stability of the method. The performance will be analyzed in Section IV-A.

D. Upscaling Method

Upscaling is used to transfer the LAI field measurements at the ESUs to the LAI reference map. The upscaling method directly affected the accuracy of the LAI reference map by extrapolation from the limited sample set to the entire site in the geographical space. The site-specific transfer function is currently the main upscaling method based on ground measurements [19]. It establishes a relationship between the average LAI values from each ESU and the corresponding high-resolution reflectance or VI. The LAI values of the sampling points from the high-resolution LAI map with Gaussian noise in Section III-C is regarded as the ground measurement value of the ESU, and we use direct pixel-by-pixel correlation. The least-squares regression method is tested on the NDVI and SR for the upscaling process, and the transfer function that has a lower RMSE is selected as the optimum function. For the Sud-Ouest site, the SR has a lower RMSE than the NDVI, so the relationship between the SR and LAI is used as the transfer function for the Sud-Ouest site. The selected transfer functions of the two sites are shown in Table III. Both methods display reasonable fitting performance, although Method 2 fits slightly better than Method 1 because it has a lower RMSE and a higher R^2. A direct comparison of the goodness of fit of the two methods may be meaningless because the R^2 and RMSE values are calculated with different sample sets. In LAI product validation, the role of the transfer function is to extrapolate from the sample set to the entire site, and whether the transfer function can be extended to the entire site is another issue that will be discussed in Sections IV-C and IV-D. A transfer function may fit well for the sample set or in a local region, but it may not perform well when it is extrapolated to the entire site.

E. Comparison of the Aggregated LAI Reference Map to the Benchmark

After the LAI reference map was obtained by applying the transfer function over the site, it was aggregated to a 1-km resolution. The original high-resolution LAI map was also aggregated to a 1-km resolution and was considered as the benchmark for the evaluation. The root mean square error (RMSE) between the aggregated LAI reference map and benchmark was calculated to represent the accuracy of the corresponding sampling strategy. To analyze the accuracy and stability of the method with increasing numbers of samples, the RMSEs were calculated for 10–100 samples at intervals of 10.

IV. ANALYSIS BASED ON THE SIMULATED IMAGES

A. Accuracy and Stability of the Two Methods

In this paper, "Method 1" is used to refer to the SSVIP approach and "Method 2" is used to refer to the sampling strategy based on vegetation types. In this section, Method 1 is compared

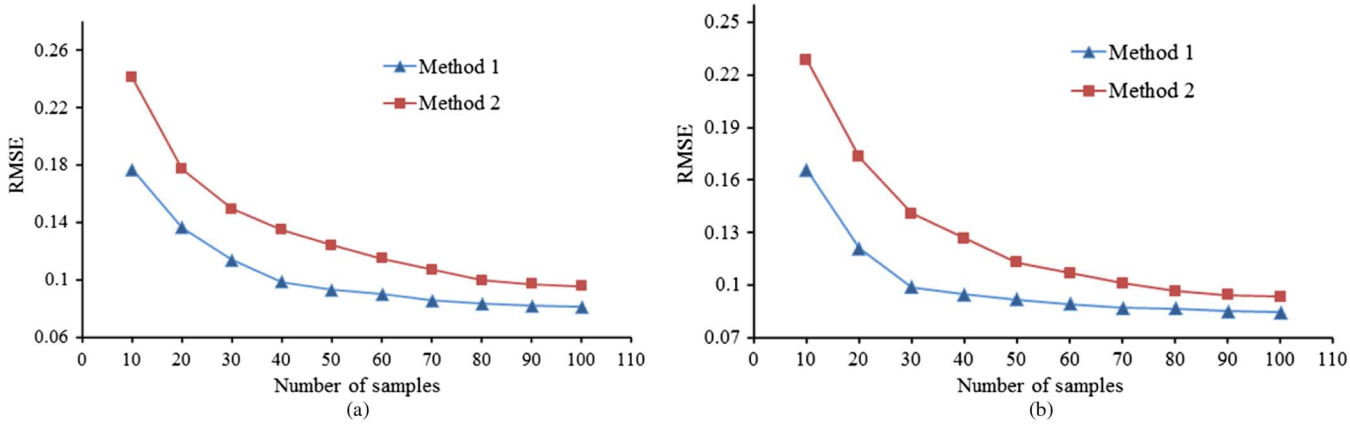

Fig. 3. Changes of RMSE in Method 1 and Method 2 with the increasing of samples number at (a) the Sud-Ouest site and (b) the Camerons site.

with Method 2 to analyze their accuracy and stability. Fig. 3 presents the change in the average RMSE in the study area with an increasing number of samples at Sud-Ouest and Camerons. The RMSE decreased with an increasing number of samples for fewer than 80 samples, whereas the RMSE values based on the two methods remained constant for more than 80 samples. The RMSE of Method 1 is always less than that of Method 2. Thus, the accuracy of both methods improves with an increasing number of samples, but Method 1 performs better than Method 2. Even when the RMSE becomes stable and reaches the optimum value, the RMSE of Method 1 is approximately 0.02 less than that of Method 2 at Sud-Ouest and 0.01 less at Camerons. Furthermore, Method 1 becomes stable more quickly than Method 2, which indicates that the samples chosen by Method 1 are more representative of the study site. Thus, the LAI reference map generated by SSVIP improves the average accuracy of the LAI reference map by at least 0.04, and the method becomes stable more quickly than the current sampling strategy.

The evaluation procedure was repeated $N = 1000$ times, and after removing the $N\alpha/2 = 25$ $(1 - \alpha = 95\%)$ highest and lowest RMSE values, the RMSE in Fig. 3 was compared with the remaining 950 RMSE values. σ is defined as the larger deviation from the RMSE in Fig. 3 from the highest and lowest values of the 950 residual RMSE series. At the Sud-Ouest site, Method 1 has deviations σ of 0.01 for 10 samples and less than 0.01 for 20–100 samples, whereas Method 2 has a deviation of 0.01 for 10 and 20 samples and deviations less than 0.01 for 30–100 samples. At the Camerons site, Method 1 has deviations σ less than 0.01 for 10–100 samples, whereas Method 2 has a deviation of 0.01 for 10 samples and deviations less than 0.01 for 20–100 samples. These results suggest that the noise associated with the data can be filtered when averaging the high-resolution reference LAI map to a 1-km resolution. Furthermore, the results are statistically representative when comparing σ with the range of RMSE values in Fig. 3.

B. Sample Number and Heterogeneity

Fig. 3 illustrates that the proposed Method 1 requires 40 samples to reach the stable accuracy of 0.1 at Sud-Ouest, whereas Method 2 requires approximately 80 samples. At Camerons, Method 1 requires approximately 30 samples to reach the stable accuracy of 0.1, whereas Method 2 requires approximately 80 samples. SSVIP always requires fewer samples than Method 2 to attain a higher accuracy. Fig. 3 also illustrates that both methods reach the stable accuracy more quickly at Camerons than at Sud-Ouest because of the different amounts of heterogeneity at the two sites.

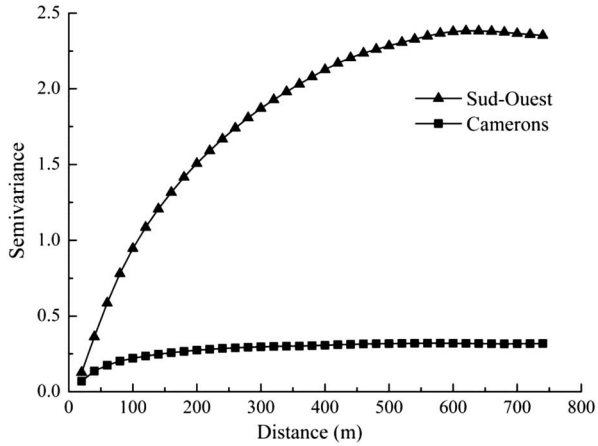

Fig. 4. Semivariance in LAI with increasing lag distance from 20 to 740 m at the Sud-Ouest site, which has an area of 3 km × 3 km, and at the Camerons site, which has an area of 4 km × 4 km.

The heterogeneity also affects the determination of the number of samples. Generally, heterogeneity is shown in the feature space and geographical space. Feature heterogeneity can be quantitatively described by the variance of the corresponding parameter. The average LAIs of the 20-m resolution LAI map are 1.96 at Sud-Ouest and 2.13 at Camerons. The minimum values of LAI at both sites are zero, whereas the maximum values are 5.65 and 4.10, respectively. The variance at Sud-Ouest is 2.15, which is significantly higher than the variance of 0.33 at Camerons. This difference in variance indicates that the vegetation is much more heterogeneous at Sud-Ouest than at Camerons.

A semivariogram was used to quantitatively describe the spatial heterogeneity in the geographical space. The semivariance $r(h)$ of Z variances between all pairs of points $Z(x)$ and $Z(x + h)$ that are separated by a distance h can be calculated as

$$r(h) = \frac{1}{2} VAR[Z(x + h) - Z(x)]. \quad (7)$$

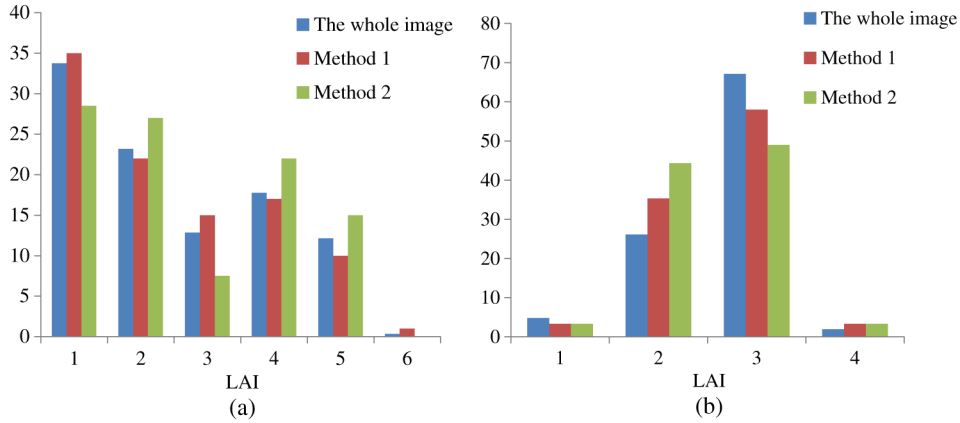

Fig. 5. LAI frequency distribution histograms of the entire site and the samples selected by the two methods. The number i on the horizontal axis represents the LAI value in the interval $[i-1, i)$. The vertical axis represents the percentage of the LAI frequency distribution in the given interval. (a) Sud-Ouest. (b) Camerons.

Fig. 4 presents the LAI variograms at the two sites. The global variance (sill) is significantly higher at Sud-Ouest than at Camerons, which indicates that the geographical space at the Sud-Ouest site is more heterogeneous than at the Camerons site. The high heterogeneity of Sud-Ouest is shown by the intermixing of the crop fields with high LAI values and the soil fields with low vegetation cover. The Camerons site mainly contains green understory and a high density of broadleaf trees, which homogenizes the LAI distribution. As a result, the broadleaf forest site is more homogeneous than the crop site at the landscape level.

Fig. 3 illustrates that the Sud-Ouest site requires more samples to attain the same accuracy than the Camerons site, although the area of the former is smaller than the latter. This finding suggests that heterogeneity is an important factor that affects the determination of the sample number. A heterogeneous site requires more samples than a homogeneous site to meet the same target accuracy.

C. Representation of ESU Samples in the Feature Space

Because the number of pixels in the ESUs is different from the entire site, the two histograms cannot be compared directly. After transforming the histograms to frequency distribution histograms at the given interval, the samples and entire site can be compared at the same standard. Fig. 5 presents the frequency distribution histograms of the LAI map and the ESUs selected by the two methods. At Sud-Ouest, intervals 0–1 and 2–3 are slightly oversampled by Method 1, whereas intervals 1–2, 3–4, and 4–5 are undersampled. Using Method 2, intervals 1–2, 3–4, and 4–5 are oversampled, whereas 0–1 and 2–3 are undersampled. The variable BIAS is used to quantitatively represent the difference between the histograms. BIAS is defined as

$$BIAS = \sum_{j=1}^{C} \left| \frac{n_j}{n} - \kappa_j \right| \tag{8}$$

where n_j is the number of samples in interval j, n is the sample size, and κ_j is the proportion of the image in interval j. At Sud-Ouest, Method 1 has a BIAS of 0.09, whereas Method 2 has a BIAS of 0.22. This finding indicates that the sample histogram generated by Method 1 is more similar to the entire image than the histogram generated by Method 2 and demonstrates that the samples selected by Method 1 can represent the entire Sud-Ouest site. At Camerons, both methods are oversampled in interval 1–2 but are undersampled in interval 2–3. The BIAS is 0.21 using Method 1 and 0.39 using Method 2, which also illustrates that the samples from Method 1 are more representative than those from Method 2.

The analysis presented above also illustrates that both methods have a higher BIAS at Camerons than at Sud-Ouest. This difference in BIAS is partly because the VI of the Camerons area is classified into four classes, whereas the Sud-Ouest side uses five classes. The method has more constraints on the feature distribution of the samples as the number of classes increases. Another possible reason for the difference in BIAS is that the stratified sampling strategy is more applicable over heterogeneous surfaces. For homogeneous surfaces, there is little helpful information in the feature space that can be utilized by the stratified strategy whether it is based on VI or vegetation type. The performance became similar to the methods that do not use stratified strategies.

D. Representation of ESU Samples in the Geographical Space

Fig. 6 presents the spatial distribution of the samples selected by the two methods at Sud-Ouest and Camerons. The background images are false color composite maps of the simulated high-resolution reflectance images. The samples selected by Method 2 at Sud-Ouest [Fig. 6(b)] are clustered on the upper-left and lower-right sides, and a considerable empty area is present on the lower-left side. This phenomenon is also present at Camerons but is slightly attenuated [Fig. 6(d)]. The samples selected by Method 1 are spread across the entire area at both sites [Fig. 6(a) and (c)]. The NNIs for Fig. 6(a), (b), (c), and (d) are 1.32, 0.99, 1.47, and 1.12, respectively. The results indicate that the samples selected by Method 2 are similar to a random distribution, whereas the samples selected by Method 1 are similar to the dispersed distribution. The sampling strategy based on the VI performs better in reducing the redundancy of the sampling information.

E. Accuracy of the LAI Reference Maps

Fig. 7 presents the degraded LAI map and the error of the LAI reference maps generated by the two methods at

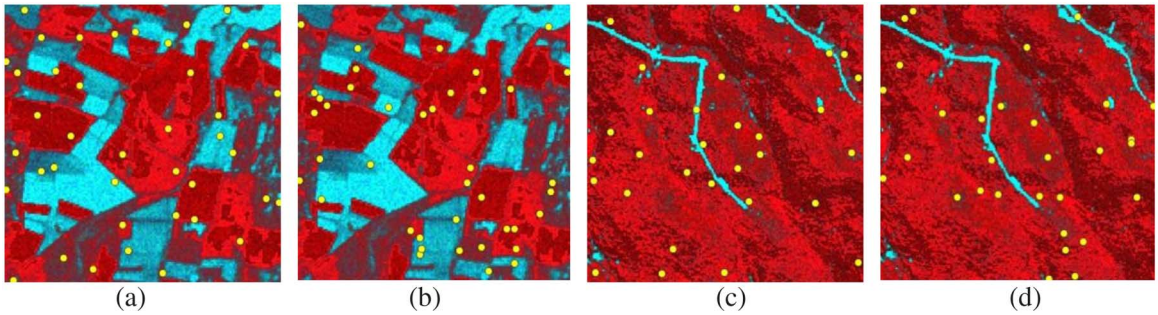

Fig. 6. Spatial distribution of samples at Sud-Ouest by (a) Method 1 and (b) Method 2, and at Camerons by (c) Method 1 and (d) Method 2.

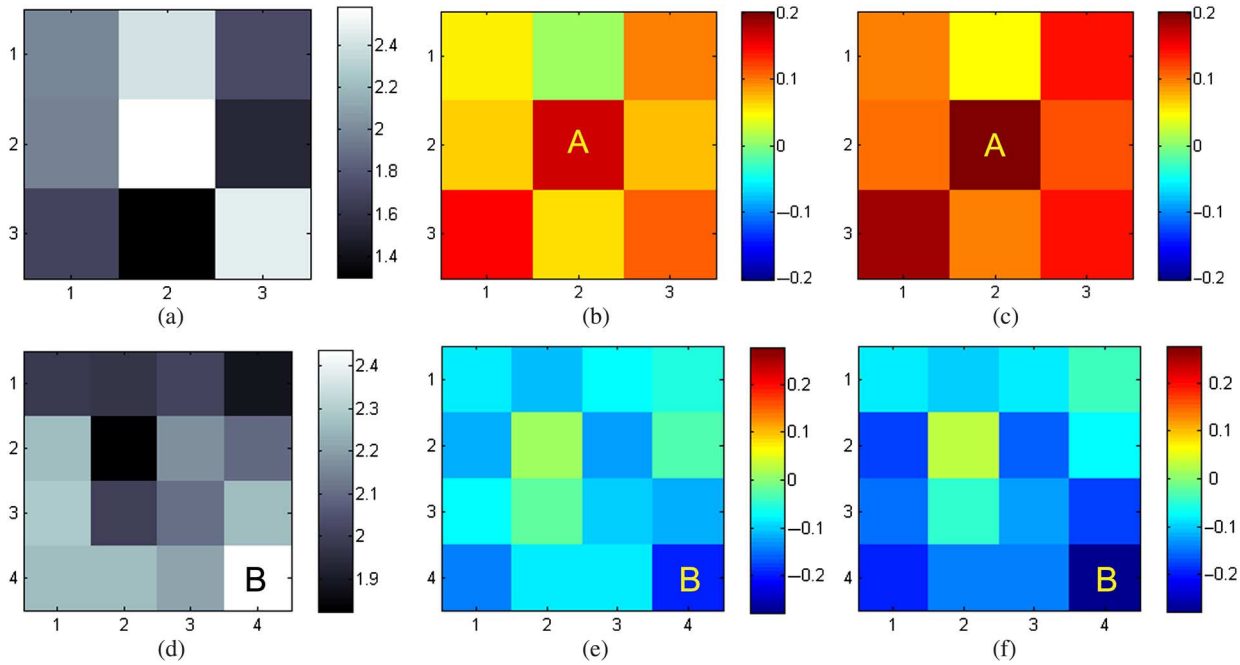

Fig. 7. Accuracy evaluation of the LAI reference maps by the two methods. The graphs illustrate the degraded LAI maps and LAI reference map error at Sud-Ouest (a)–(c) and at Camerons (d)–(f) by Method 1 and Method 2. (a) Degraded LAI map. (b) LAI reference map error by Method 1. (c) LAI reference map error by Method 2 at the Sud-Ouest site. (d) Degraded LAI map. (e) LAI reference map error by Method 1. (f) LAI reference map error by Method 2 at the Camerons site.

Sud-Ouest and Camerons based on the framework described in Fig. 1 and Section III. At the Sud-Ouest site, the RMSEs from Methods 1 and 2 are 0.10 and 0.14, respectively. The maximum BIAS values are 0.17 for Method 1 and 0.20 for Method 2. At the Camerons site, the RMSEs are 0.10 for Method 1 and 0.14 for Method 2, and the maximum biases are 0.19 and 0.28, respectively. Method 1 outperforms Method 2 at both sites.

The sampling strategy is a key factor that affects the accuracy of the LAI reference map. The spatial sampling strategy determines which samples can represent the site in terms of the features and the spatial distribution. These samples determine the coefficients of the transfer function, which will ultimately affect the accuracy of the LAI reference map in the validation procedure. Therefore, an efficient sampling strategy must cover the entire range of LAI values and have good coverage of the area, an accurate estimation of the LAI, and good spatial representativeness of the entire site. Consequently, an accurate and robust transfer function that accurately represents the site can be established.

Even under the same sampling strategy, the error caused by different medium-resolution pixels can vary considerably (Fig. 7). For a given sample dataset, the prediction error is affected by the difference between the sample and pixel mean ($|\bar{X} - \bar{x}|$) and the heterogeneity of the pixel (S_x) when MSE, n, $\bar{x}$, and s_x are fixed.

The pixels with relatively high LAI values typically have larger errors (Fig. 7). For example, pixels A and B have the largest LAI at Sud-Ouest (2.58) and at Camerons (2.44), respectively, and both have the maximum bias from the two methods (0.17 and −0.19 for Method 1, 0.20 and −0.28 for Method 2). This result can be explained by (1), where a higher LAI value of a pixel is more likely to yield a larger value of $|\bar{X} - \bar{x}|$ when MSE, n, $\bar{x}$, and s_x are fixed. However, for a given sampling strategy, the influence of a high LAI value on the prediction error may be compensated for by low heterogeneity within the pixel, which can cause the error to be small. According to (1), the prediction error of a pixel is a complex interaction between the LAI, heterogeneity, and transfer function for a given sampling strategy.

TABLE IV
DATASET OF THE 24 VALERI VALIDATION SITES (THE DETAILED INFORMATION CAN BE FOUND AT http://w3.avignon.inra.fr/valeri/)

Site	Land cover	Date	Lat.	Lon.	$m_{Pop.}$	$\sigma_{Pop.}$	m_{SSVIP}	σ_{SSVIP}	m_{VALERI}	σ_{VALERI}	NNI_{SSVIP}	NNI_{VALERI}
Haouz	Cropland	03/2003	31.66	–7.6	0.480	0.176	0.481	0.179	0.479	0.174	1.69	0.76
Romilly-sur -Seine	Cropland	06/2000	48.44	3.77	0.623	0.113	0.621	0.124	0.662	0.087	1.57	1.10
Alpilles	Cropland	07/2002	43.81	4.71	0.440	0.181	0.439	0.184	0.512	0.163	1.69	1.22
Plan-de-Dieu	Cropland	07/2004	44.2	4.95	0.254	0.070	0.253	0.069	0.248	0.075	1.67	1.30
Demmin	Cropland	06/2004	53.89	13.21	0.472	0.140	0.472	0.142	0.469	0.144	1.69	0.66
Fundulea	Cropland	05/2001	44.41	26.58	0.619	0.230	0.620	0.234	0.749	0.183	1.86	0.71
Barrax	Cropland	07/2003	39.07	–2.1	0.280	0.190	0.280	0.191	0.465	0.186	1.65	0.41
Chilbolton	Crops and forest	06/2006	51.16	–1.43	0.779	0.150	0.781	0.146	0.763	0.149	1.66	0.57
Gilching	Crops and forest	07/2002	48.08	11.32	0.598	0.121	0.599	0.121	0.644	0.123	1.79	1.01
Aek Loba	Broad leaf forest	05/2001	2.63	99.58	0.654	0.037	0.654	0.033	0.661	0.020	1.74	0.97
Puéchabon	Broad leaf forest	06/2001	43.72	3.65	0.529	0.092	0.528	0.095	0.532	0.077	1.59	0.62
Sierra Chincua	Needle leaf forest	12/2001	19.67	–100.28	0.733	0.055	0.733	0.054	0.749	0.044	1.80	1.24
Sonian	Needle leaf forest	06/2004	50.77	4.41	0.639	0.090	0.633	0.115	0.665	0.037	1.68	0.57
Järvselja	Needle leaf forest	04/2007	58.3	27.26	0.520	0.070	0.521	0.069	0.541	0.060	1.69	0.93
Hirsikangas	Needle leaf forest	08/2003	62.64	27.01	0.598	0.094	0.597	0.091	0.612	0.075	1.71	1.10
Rovaniemi	Needle leaf forest	06/2004	66.45	25.35	0.627	0.051	0.626	0.052	0.618	0.053	1.81	0.86
Nezer	Needle leaf forest	06/2001	44.47	–1.04	0.614	0.106	0.615	0.101	0.641	0.053	1.56	0.16
Larose	Mixed forest	08/2003	45.38	–75.22	0.701	0.059	0.703	0.052	0.710	0.043	1.70	1.24
Concepción	Mixed forest	01/2003	–37.47	–73.47	0.689	0.089	0.690	0.086	0.663	0.121	1.67	1.22
Wankama	Grassland	06/2005	13.64	2.64	0.113	0.015	0.114	0.017	0.116	0.014	1.68	0.41
Laprida	Grassland	11/2001	–36.99	–60.55	0.622	0.093	0.622	0.089	0.593	0.091	1.75	1.00
Zhang Bei	Grassland	08/2002	41.28	114.69	0.435	0.113	0.432	0.117	0.454	0.102	1.67	1.32
Larzac	Grassland	07/2002	43.94	3.12	0.485	0.060	0.483	0.057	0.474	0.055	1.80	1.37
Turco	Shrubland	08/2002	–18.24	–68.19	0.110	0.013	0.110	0.012	0.107	0.010	1.72	1.17

Date is the LAI field campaign time. $m_{Pop.}$ and $\sigma_{Pop.}$ are the mean and standard deviation of the NDVI images, respectively. m_{SSVIP} and m_{VALERI} are the mean NDVI of the ESUs selected by SSVIP and the VALERI campaign, respectively. σ_{SSVIP} and σ_{VALERI} are the NDVI standard deviations of the ESUs selected by SSVIP and the VALERI campaign, respectively. NNI_{SSVIP} and NNI_{VALERI} are the NNI of the ESUs selected by SSVIP and the VALERI campaign, respectively.

V. ANALYSIS BASED ON THE VALERI DATASET

The advantage of the analysis based on simulated images is that the accuracy and stability of the sampling strategy can be analyzed using the provided LAI base map as the true values. However, the simulated heterogeneous characteristics are limited due to the lack of information about parameters at the study site other than the LAI, such as leaf chlorophyll, water content, and soil reflectance, which can impact the results. The VALERI field campaign established a global network of LAI observation sites that cover a wide range of vegetation types. The dataset has been widely used in LAI product validation studies [21], [34], [48]. The sampling strategy in the VALERI project was mainly based on vegetation types [32]. Thus, SSVIP was applied to 24 actual validation sites from the VALERI dataset and was compared with the sampling strategy used in the VALERI project. Because of the lack of true LAI measurements, only those values representative of ESUs from different sampling strategies in the feature space and geographical space were analyzed.

A. Site Description and Heterogeneity Analysis

The VALERI project includes 24 actual validation sites (Table IV), and corresponding 20-m resolution SPOT-HRV images were acquired several days before or after the LAI field measurements were taken. Radiance calibration was performed on all of the images, and the images were georeferenced to the UTM/WGS84 projection. No atmospheric correction was applied because all of the images are cloud free, and it is safe to assume that the effect of the atmosphere was identical over the validation sites [19]. NDVI images of the 24 validation sites were generated using the SPOT-HRV images.

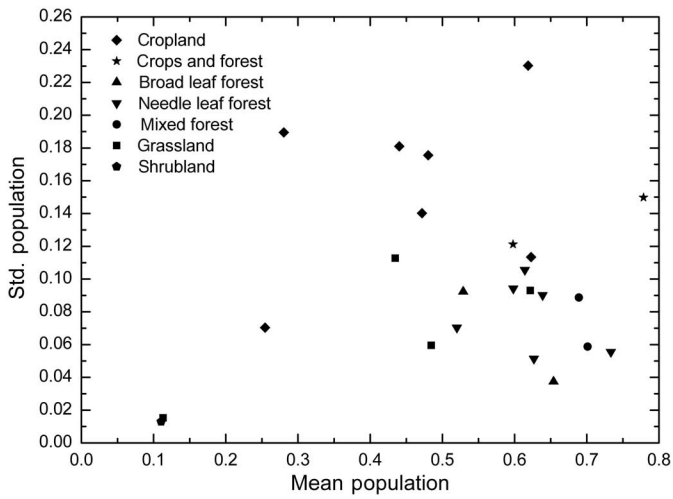

Fig. 8. Mean and standard deviation of the NDVI images at the 24 VALERI validation sites for a total of seven vegetation types.

Fig. 8 compares the mean (m_{pop}) and standard deviation (σ_{pop}) of the NDVI images of the 24 validation sites. The results suggest that the cropland sites have medium vegetation cover (m ranges from 0.280 to 0.619) and are the most heterogeneous sites (σ ranges from 0.113 to 0.230) except for Plan-de-Dieu. This finding is due to the intermixing of crop fields with high NDVIs and bare soil with low NDVIs. The Plan-de-Dieu site has the lowest heterogeneity (σ is 0.070) of the cropland sites; the vegetation cover in the crop fields is relatively low (m equals 0.254), which decreases the NDVI variability between the crop fields and bare soil fields. In contrast, forest sites have the highest vegetation cover (m ranges from 0.520 to 0.733) but are more

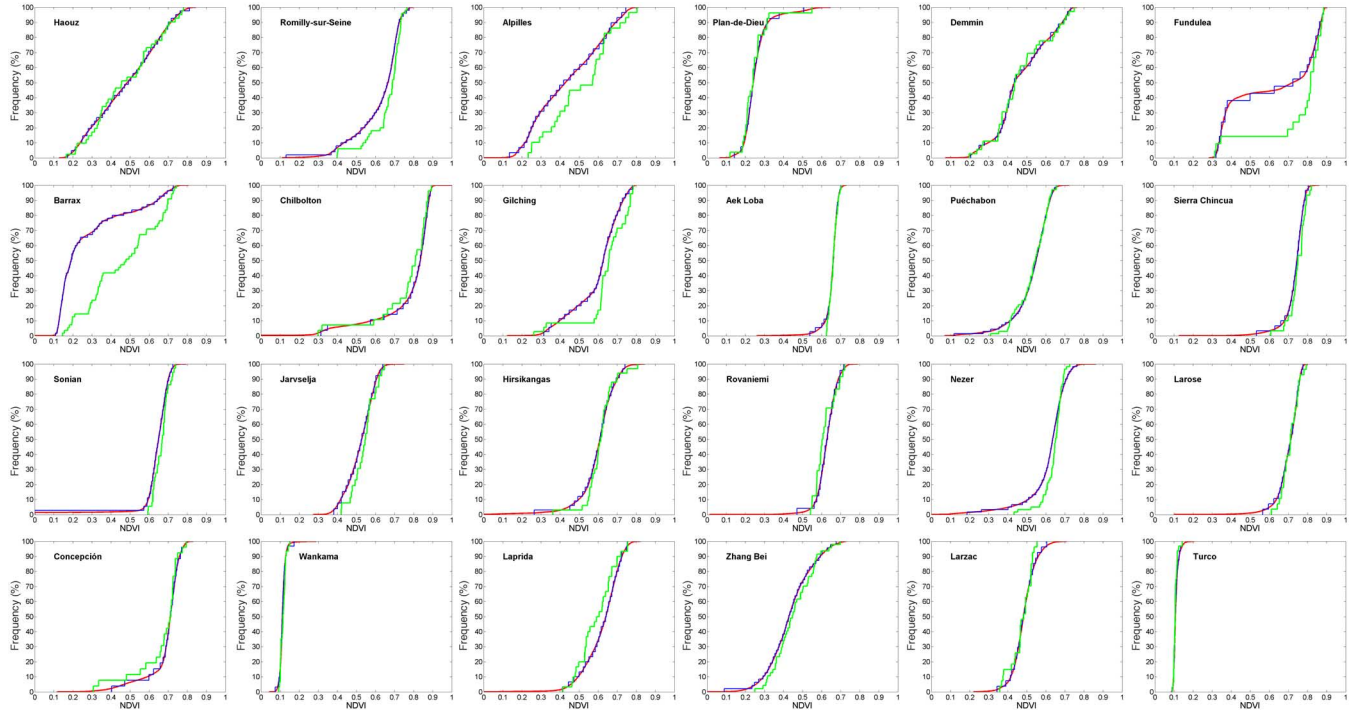

Fig. 9. NDVI cumulative frequency distributions of the ESUs selected by SSVIP (blue) and by the VALERI campaign (green), and the NDVI cumulative frequency distribution over the entire image (red) at the 24 VALERI validation sites.

homogeneous than cropland sites (σ ranges from 0.037 to 0.106). The source of the heterogeneity was the presence of nonvegetated areas (roads and open areas), such as in Nezer and Puéchabon, and the mixed distribution of cropland and forest, such as in Chilbolton. Grassland sites, also have medium vegetation cover levels similar to the cropland sites, but they are more homogeneous, with σ values of less than 0.113. This analysis demonstrates that the cropland sites typically have the highest heterogeneity, whereas the natural vegetation areas, such as forest, grassland, and shrubland sites, have lower variability at the 24 VALERI sites.

B. Representative Analysis

The location of each ESU in the VALERI sites was provided in the VALERI campaign reports [32]. The number of ESUs for each vegetation type was generally proportional to the area of that type [32]. The generated NDVI images of the 24 validation sites were used as *a priori* knowledge in SSVIP to determine the distribution of the ESUs. To allow for a comparison with the VALERI project, the number of ESUs at each site in SSVIP was set to be the same as that in the VALERI campaign reports. As discussed in Step 3 in Section II-B, the number of strata was set equal to the number of ESUs to achieve the highest efficiency. The optimal segmentation threshold was determined by the OF in (2), and the optimum sample set was selected by NNI, as discussed in Section II-B.

The representation of the ESUs in the feature space was evaluated. Fig. 9 presents the NDVI cumulative frequency distribution of the ESUs selected by SSVIP and by the VALERI campaign as well as the NDVI distribution over the entire image at the 24 validation sites. The NDVI distribution of the ESUs selected by SSVIP is more consistent with that of the entire image than that given by the VALERI campaign at most of the sites. Fig. 10 compares the means and standard deviations of the ESUs selected by the two methods and the entire image. The difference between the mean NDVI of the ESUs selected by SSVIP and that of the entire image is within 0.006 for all 24 validation sites, suggesting that the ESUs selected by SSVIP are unbiased and are well represented in the feature space. Figs. 9 and 10(a) illustrate that at Barrax, Fundulea, and Alpilles, the ESUs selected by the VALERI campaign are largely oversampled in areas with high NDVIs; this oversampling is caused by the difference of 0.07 between the mean NDVI of the ESUs and the population. At Barrax, areas with NDVI values lower than 0.12, between 0.21 and 0.29, and between 0.35 and 0.42 were not sampled. At Fundulea, areas with NDVI values lower than 0.33 and between 0.34 and 0.69 were not sampled. At Gilching, Romilly-sur-Seine, Nezer, Sonian, and Järvselja, the ESUs are slightly oversampled in high-NDVI areas. At Gilching, areas with NDVI values between 0.33 and 0.57 were not sampled. At Laprida, Concepción and Chilbolton, the ESUs are slightly undersampled in areas of high NDVI. Fig. 10(b) illustrates that at Fundulea, Sonian and Nezer, the standard deviations of the ESUs selected by the VALERI campaign are clearly less than those of the entire image, indicating that the ESUs were clustered and not spread across the feature space. This analysis illustrates that the ESUs selected by SSVIP are more representative of the feature space than the sampling strategy in the VALERI campaign.

The representation of the ESUs in the geographical space was then evaluated. Fig. 11 compares the NNIs of the ESUs selected by the two methods. According to the definition of NNI, values greater than one indicate a dispersed distribution. The NNI values from SSVIP are greater than 1.55 at all 24 validation

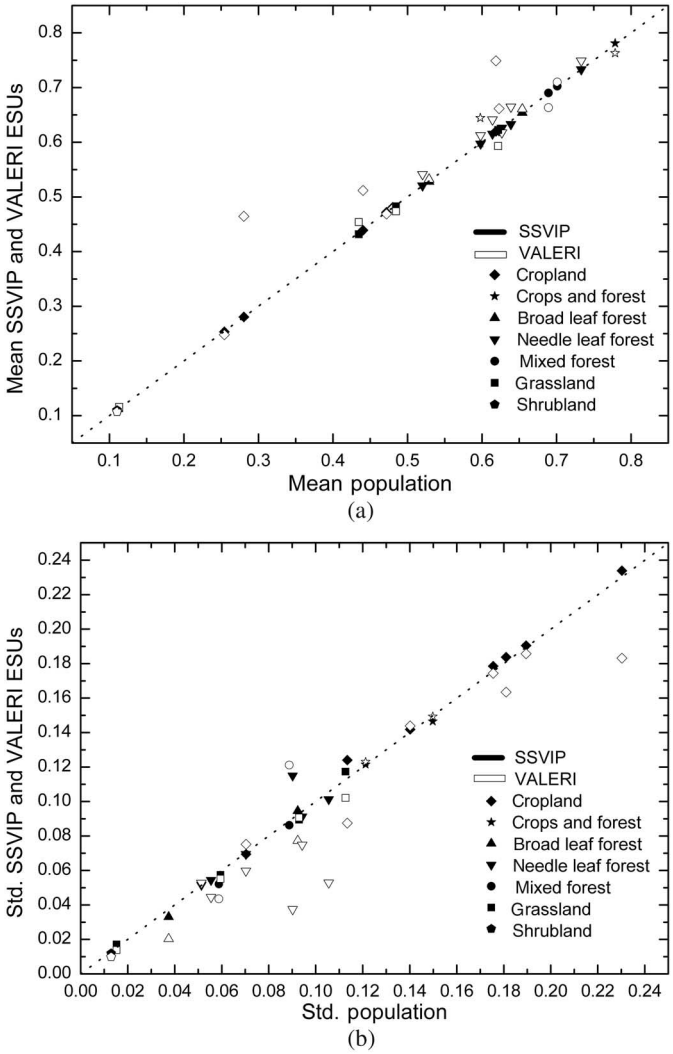

Fig. 10. NDVI (a) mean and (b) standard deviations of the ESUs selected by two methods (SSVIP and VALERI campaign) and the entire image at 24 VALERI validation sites for a total of seven vegetation types.

sites, whereas the NNI values at 13 sites from the VALERI campaign are less than one. The NNI values from SSVIP are higher than those from the VALERI campaign at all of the validation sites. This result indicates that the ESUs from SSVIP are well dispersed and have good coverage across the geographical space. The NNI values at Nezer, Barrax, and Wankama are less than 0.5, which indicates strong spatial clustering.

This analysis illustrates that SSVIP is more representative in both the feature and geographical spaces than the sampling strategy in the VALERI campaign. In the VALERI project, the corresponding SPOT images of the validation sites were acquired several days before or after the LAI field measurements were taken. Because the image was not acquired when the field measurements were taken, the image used in analysis is the same as that used as *a priori* knowledge, which is why the ESUs selected by SSVIP are consistent with the population of the entire site. This result also demonstrates that SSVIP can perform well if the NDVI map used as *a priori* knowledge is similar to that acquired when the experiment was performed.

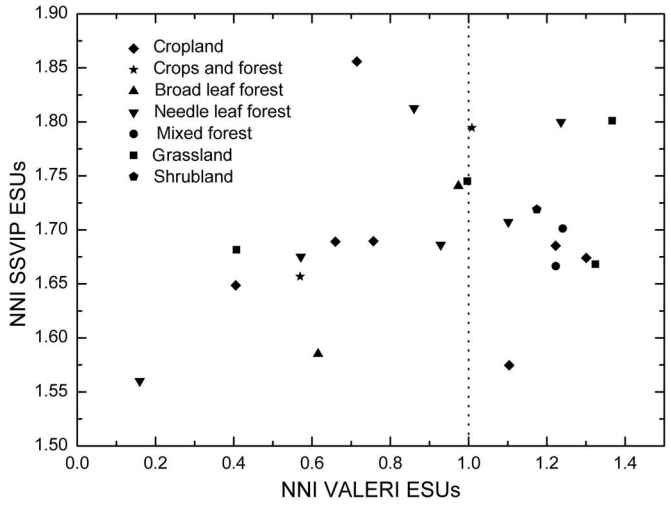

Fig. 11. Evaluation of the ESUs representation in the geographical space. Comparison of the NNI of the ESUs selected by SSVIP and by the VALERI campaign at 24 VALERI validation sites. According to the definition of the NNI, an NNI greater than one indicates a dispersed distribution, whereas an NNI less than one indicates aggregation.

VI. Conclusion

We developed a spatial sampling strategy (SSVIP) using a high-resolution VI map for LAI product validation over heterogeneous surfaces based on a bottom-up validation framework. Compared with the widely used sampling strategy based on vegetation types, SSVIP is more suitable for sampling over heterogeneous areas. In theory, with the bottom-up validation framework, the choice of the prior knowledge for the stratified sampling method is affected by the method used to build the transfer function. A uniform empirical relationship between the LAI and the reflectance or VI is widely used to build the transfer function. Therefore, the VI, which is related to the vegetation growth stage, is most suitable as *a priori* knowledge. The results also demonstrate that SSVIP has good performance in the following areas: 1) the LAI reference map from SSVIP is more accurate and stable than that from the sampling strategy based on vegetation types; 2) SSVIP requires fewer samples to become stable and has higher accuracy; and 3) the samples from SSVIP are spread across the feature space and the geographical space. These improvements generate an accurate LAI reference map and reasonable validation over heterogeneous areas for coarse- and moderate-resolution LAI products.

An NDVI map acquired in advance is needed as *a priori* knowledge for SSVIP. The analysis in Section V-B illustrates that SSVIP can perform well if the NDVI map used as *a priori* knowledge has smaller differences than that acquired when the experiment was performed. The NDVI map is important for the application of the SSVIP. In some regions, the NDVI map can be obtained close to the time of the field campaign due to the coverage of high-temporal-resolution and high-spatial-resolution satellites. For example, the satellite HJ-1A/1B, which was launched by China in 2009, has a revisit cycle of two days and a 30-m resolution attained by satellite networking and only covers China. However, there may be a long interval between the acquisition time of the VI map and the field measurements in

some regions. In this case, SSVIP could be used as well if the vegetation growth is stable and there are only small variations in the heterogeneity of the region. The application of SSVIP is limited if the vegetation is rapidly increasing or decreasing.

The aim of SSVIP is to improve the accuracy of the LAI reference map and to improve the representation of ESUs. In practice, the feasibility of performing an experiment at the locations of the chosen ESUs and other factors, such as manpower, should be considered. For example, some ESUs may be located in the mountainous areas, where it is difficult to perform experiments. This problem could be solved by excluding the areas that cannot be reached. The other deficiency of SSVIP is that there is no universal method to quantitatively determine the number of samples by considering the site area and heterogeneity. The analysis in this paper illustrates that the heterogeneity characteristics of the sampling area have a clear influence on the number of samples. Further research is necessary to overcome these deficiencies. The other research direction is to combine the VI and vegetation types as *a priori* knowledge. The transfer function should consider the vegetation type as well. Both of these items will further improve the accuracy of the LAI reference map and LAI ground validation data.

Acknowledgment

The authors thank the VALERI project for data support and the anonymous reviewers for their insightful comments and suggestions.

References

[1] G. B. Bonan, "Importance of leaf area index and forest type when estimating photosynthesis in boreal forests," *Remote Sens. Environ.*, vol. 43, pp. 303–314, 1993.

[2] J. Clevers, C. Büker, H. Van Leeuwen, and B. Bouman, "A framework for monitoring crop growth by combining directional and spectral remote sensing information," *Remote Sens. Environ.*, vol. 50, pp. 161–170, 1994.

[3] P. C. Doraiswamy, T. R. Sinclair, S. Hollinger, B. Akhmedov, A. Stern, and J. Prueger, "Application of MODIS derived parameters for regional crop yield assessment," *Remote Sens. Environ.*, vol. 97, pp. 192–202, 2005.

[4] W. Yang, D. Huang, B. Tan, J. C. Stroeve, N. V. Shabanov, Y. Knyazikhin *et al.*, "Analysis of leaf area index and fraction of PAR absorbed by vegetation products from the terra MODIS sensor: 2000–2005," *IEEE Trans. Geosci. Remote Sens.*, vol. 44, no. 7, pp. 1829–1842, Jul. 2006.

[5] F. Baret, O. Hagolle, B. Geiger, P. Bicheron, B. Miras, M. Huc, B. Berthelot, F. Niño, M. Weiss, O. Samain, J. L. Roujean, and M. Leroy, "LAI, fAPAR and fCover CYCLOPES global products derived from VEGETATION: Part 1: Principles of the algorithm," *Remote Sens. Environ.*, vol. 110, pp. 275–286, 2007.

[6] C. Bacour, F. Baret, D. Beal, M. Weiss, and K. Pavageau, "Neural network estimation of LAI, fAPAR, fCover and LAIxCab, from top of canopy MERIS reflectance data: Principles and validation," *Remote Sens. Environ.*, vol. 105, pp. 313–325, 2006.

[7] Y. Knyazikhin, J. Martonchik, R. Myneni, D. Diner, and S. Running, "Synergistic algorithm for estimating vegetation canopy leaf area index and fraction of absorbed photosynthetically active radiation from MODIS and MISR data," *J. Geophys. Res. Atmos. (1984–2012)*, vol. 103, pp. 32257–32275, 1998.

[8] S. Ganguly, A. Samanta, M. A. Schull, N. V. Shabanov, C. Milesi, R. R. Nemani, Y. Knyazikhin, and R. B. Myneni, "Generating vegetation leaf area index earth system data record from multiple sensors. Part 2: Implementation, analysis and validation," *Remote Sens. Environ.*, vol. 112, pp. 4318–4332, 2008.

[9] S. Ganguly, M. A. Schull, A. Samanta, N. V. Shabanov, C. Milesi, R. R. Nemani, Y. Knyazikhin, and R. B. Myneni, "Generating vegetation leaf area index earth system data record from multiple sensors. Part 1: Theory," *Remote Sens. Environ.*, vol. 112, pp. 4333–4343, 2008.

[10] D. Huang, W. Yang, B. Tan, M. Rautiainen, Z. Ping, H. Jiannan *et al.*, "The importance of measurement errors for deriving accurate reference leaf area index maps for validation of moderate-resolution satellite LAI products," *IEEE Trans. Geosci. Remote Sens.*, vol. 44, no. 7, pp. 1866–1871, Jul. 2006.

[11] B. Hu, J. R. Miller, J. M. Chen, and A. Hollinger, "Retrieval of the canopy leaf area index in the BOREAS flux tower sites using linear spectral mixture analysis," *Remote Sens. Environ.*, vol. 89, pp. 176–188, 2004.

[12] J. Campbell, S. Burrows, S. Gower, and W. Cohen, (2012, Nov. 12). *BigFoot Field Manual*, version 2.1 [EB/OL][Online]. Available: http://www.fsl.orst.edu/larse/bigfoot/index.html accessed on 1999.

[13] W. B. Cohen, T. K. Maiersperger, and D. Pflugmacher, (2013, Nov. 2). *BigFoot Leaf Area Index Surfaces for North and South American Sites, 2000–2003. Data Set.* Oak Ridge, TN, USA: Oak Ridge National Laboratory Distributed Active Archive Center [Online]. Available: http://www.daac.ornl.gov. accessed on 2006.

[14] W. Buermann and M. Helmlinger, (2013, Nov. 28). *SAFARI 2000LAI and FPAR Measurements at Sua Pan, Botswana, Dry Season 2000 [EB/OL]*, [Online]. Available: http://daac.ornl.gov//S2 K/safari.shtml accessed on 2004.

[15] X. Li, X. Li, Z. Li, M. Ma, J. Wang, Q. Xiao, Q. Liu, T. Che, E. Chen, and G. Yan, "Watershed allied telemetry experimental research," *J. Geophys. Res. Atmos. (1984–2012)*, vol. 114, p. D22103, 2009.

[16] K. Nackaerts, P. Coppin, B. Muys, and M. Hermy, "Sampling methodology for LAI measurements with LAI-2000 in small forest stands," *Agric. Forest Meteorol.*, vol. 101, pp. 247–250, 2000.

[17] K. Whitford, I. Colquhoun, A. Lang, and B. Harper, "Measuring leaf area index in a sparse eucalypt forest: A comparison of estimates from direct measurement, hemispherical photography, sunlight transmittance and allometric regression," *Agric. Forest Meteorol.*, vol. 74, pp. 237–249, 1995.

[18] J. M. Chen, G. Pavlic, L. Brown, J. Cihlar, S. Leblanc, H. White, R. Hall, D. Peddle, D. King, J. Trofymow, E. Swift, J. Van der Sanden, and P. Pellikka, "Derivation and validation of Canada-wide coarse-resolution leaf area index maps using high-resolution satellite imagery and ground measurements," *Remote Sens. Environ.*, vol. 80, pp. 165–184, 2002.

[19] J. T. Morisette, F. Baret, J. L. Privette, R. B. Myneni, J. E. Nickeson, S. Garrigues *et al.*, "Validation of global moderate-resolution LAI products: A framework proposed within the CEOS land product validation subgroup," *IEEE Trans. Geosci. Remote Sens.*, vol. 44, no. 7, pp. 1804–1817, Jul. 2006.

[20] Y. L. Zeng, J. Li, and Q. H. Liu, "Global LAI ground validation dataset and product validation framework: A review," *Adv. Earth Sci.*, vol. 27, pp. 165–174, 2012.

[21] B. Tan, J. Hu, P. Zhang, D. Huang, N. Shabanov, M. Weiss, Y. Knyazikhin, and R. B. Myneni, "Validation of moderate resolution imaging spectroradiometer leaf area index product in croplands of Alpilles, France," *J. Geophys. Res.*, vol. 110, p. D01107, 2005.

[22] R. Haining, *Spatial Data Analysis: Theory and Practice.* Cambridge, U.K.: Cambridge Univ. Press, 2003.

[23] S. Liang, *Quantitative Remote Sensing of Land Surfaces.* vol. 23. Hoboken, NJ, USA: Wiley, 2005.

[24] P. M. Rich, D. B. Clark, D. A. Clark, and S. F. Oberbauer, "Long-term study of solar radiation regimes in a tropical wet forest using quantum sensors and hemispherical photography," *Agric. Forest Meteorol.*, vol. 65, pp. 107–127, 1993.

[25] A. Stein, F. Van der Meer, and B. Gorte, *Spatial Statistics for Remote Sensing.* Norwell, MA, USA: Kluwer, 1999.

[26] B. Law, S. Van Tuyl, A. Cescatti, and D. Baldocchi, "Estimation of leaf area index in open-canopy ponderosa pine forests at different successional stages and management regimes in Oregon," *Agric. Forest Meteorol.*, vol. 108, pp. 1–14, 2001.

[27] B. Minasny and A. B. McBratney, "A conditioned Latin hypercube method for sampling in the presence of ancillary information," *Comput. Geosci.*, vol. 32, pp. 1378–1388, 2006.

[28] L. Yang, A.-X. Zhu, F. Qi, C. Z. Qin, B. Li, and T. Pei, "An integrative hierarchical stepwise sampling strategy for spatial sampling and its application in digital soil mapping," *Int. J. Geogr. Inf. Sci.*, vol. 27, pp. 1–23, 2013.

[29] V. Mulder, S. de Bruin, and M. Schaepman, "Representing major soil variability at regional scale by constrained latin hypercube sampling of remote sensing data," *Int. J. Appl. Earth Observ. Geoinf.*, vol. 21, pp. 301–310, 2013.

[30] Y. Tian, C. E. Woodcock, Y. Wang, J. L. Privette, N. V. Shabanov, L. Zhou, Y. Zhang, W. Buermann, J. Dong, B. Veikkanen, T. Hame, M. Ozdogan, Y. Knyazikhin, and R. B. Myneni, "Multiscale analysis and validation of the MODIS LAI product: II. Sampling strategy," *Remote Sens. Environ.*, vol. 83, pp. 431–441, 2002.

[31] B. Martinez, F. García-Haro, and F. Camacho-de Coca, "Derivation of high-resolution leaf area index maps in support of validation activities: Application to the cropland Barrax site," *Agric. Forest Meteorol.*, vol. 149, pp. 130–145, 2009.
[32] F. Baret, M. Weiss, D. Allard, S. Garrigues, M. Leroy, H. Jeanjean, R. Fernandes, R. Myneni, J. Privette, J. Morisette, H. Bohbot, R. Bosseno, G. Dedieu, C. Bella, B. Duchemin, M. Espana, V. Gond, X. F. Gu, D. Guyon, C. Lelong, P. Maisongrande, E. Mougin, T. Nilson, F. Veroustraete, and R. Vintilla, (2012, Dec. 7). *VALERI: A Network of Sites and a Methodology for the Validation of Medium Spatial Resolution Land Satellite Products [EB/OL]*, [Online]. Available: http://w3.avignon.inra.fr/valeri/, accessed on 2005.
[33] S. Jacquemoud, W. Verhoef, F. Baret, C. Bacour, P. J. Zarco-Tejada, G. P. Asner, C. François, and S. L. Ustin, "PROSPECT+ SAIL models: A review of use for vegetation characterization," *Remote Sens. Environ.*, vol. 113, pp. S56–S66, 2009.
[34] W. Yang, B. Tan, D. Huang, M. Rautiainen, N. V. Shabanov, Y. Wang *et al.*, "MODIS leaf area index products: From validation to algorithm improvement," *IEEE Trans. Geosci. Remote Sens.*, vol. 44, no. 7, pp. 1885–1898, Jul. 2006.
[35] T. Hengl, D. G. Rossiter, and A. Stein, "Soil sampling strategies for spatial prediction by correlation with auxiliary maps," *Soil Res.*, vol. 41, pp. 1403–1422, 2003.
[36] S. Garrigues, D. Allard, F. Baret, and M. Weiss, "Quantifying spatial heterogeneity at the landscape scale using variogram models," *Remote Sens. Environ.*, vol. 103, pp. 81–96, 2006.
[37] D. J. Brus and G. Heuvelink, "Optimization of sample patterns for universal kriging of environmental variables," *Geoderma*, vol. 138, pp. 86–95, 2007.
[38] W. G. Cochran, *Sampling Techniques.* Hoboken, NJ, USA: Wiley, 2007.
[39] D. Huang, Y. Knyazikhin, W. Wang, D. W. Deering, P. Stenberg, N. Shabanov, B. Tan, and R. B. Myneni, "Stochastic transport theory for investigating the three-dimensional canopy structure from space measurements," *Remote Sens. Environ.*, vol. 112, pp. 35–50, 2008.
[40] P. J. Clark and F. C. Evans, "Distance to nearest neighbor as a measure of spatial relationships in populations," *Ecology*, vol. 35, pp. 445–453, 1954.
[41] P. Rossello, M. Weiss, and F. Baret, (2012, Nov. 12). *Valeri 2002: Sud-Ouest Site. Ground Data Processing & Production of the Level 1 High Resolution Maps [EB/OL]*, [Online]. Available: http://www.avignon.inra.fr/valeri/, accessed on 2005.
[42] P. Rossello and M. Weiss, (2012, Nov. 12). *Valeri 2004: Camerons Site. Ground Data Processing & Production of the Level 1 High Resolution Maps [EB/OL]*, [Online]. Available: http://www.avignon.inra.fr/valeri/ accessed on 2007.
[43] J. Wang, L. Zhang, Q. Liu, B. Zhang, and Q. Yin, *A Spectrum Knowledge Base for Typical Land Surface Objects in China (in Chinese).* Beijing, China: Science Press, 2009.
[44] N. S. Goel and D. E. Strebel, "Simple beta distribution representation of leaf orientation in vegetation canopies," *Agron. J.*, vol. 76, pp. 800–802, 1984.
[45] E. Vermote, (2000). "Product accuracy/uncertainty: MOD09, surface reflectance; atmospheric correction algorithm product," *MODIS data products catalog (EOS AM Platform) [EB/OL]*, [Online]. Available: http://modarch.gsfc.nasa.gov/MODIS/RESULTS/DATAPROD/.
[46] M. Weiss, F. Baret, G. Smith, I. Jonckheere, and P. Coppin, "Review of methods for in situ leaf area index (LAI) determination: Part II. Estimation of LAI, errors and sampling," *Agric. Forest Meteorol.*, vol. 121, pp. 37–53, 2004.
[47] T. Majasalmi, M. Rautiainen, P. Stenberg, and H. Rita, "Optimizing the sampling scheme for LAI-2000 measurements in a boreal forest," *Agric. Forest Meteorol.*, vol. 154, pp. 38–43, 2012.
[48] H. Fang, S. Wei, and S. Liang, "Validation of MODIS and CYCLOPES LAI products using global field measurement data," *Remote Sens. Environ.*, vol. 119, pp. 43–54, 2012.

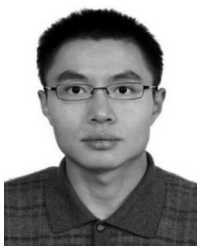

Yelu Zeng received the B.S. degree in remote sensing from Wuhan University, Wuhan, China, in 2011. He is currently pursing the Ph.D. degree at the University of Chinese Academy of Sciences, Beijing, China.

His research interests include radiative transfer modeling, validation and uncertainty analysis of remotely sensed LAI product, and LAI reversion methods.

Jing Li received the B.S. degree in geology from Zhejiang University, Hangzhou, China, in 2002, and the Ph.D. degree in cartography and geographic information system from the Graduate University of the Chinese Academy of Sciences, Beijing, China, in 2007.

She is currently an Associate Professor at the Institute of Remote Sensing and Digital Earth, Chinese Academy of Sciences (CAS), Beijing, China. She was a Visiting Scholar in Wageningen University, Wageningen, The Netherlands, in 2008–2009. Her research interests include optical radiative transfer modeling, vegetation parameter inversion methods from remote sensing, and agricultural application of remote sensing.

Qinhuo Liu received the B.Sc. degree in hydrogeology and engineering geology from Southwest Jiaotong University, Leshan, China, in 1988, the M.Sc. degree in cartography and remote sensing, in 1994, and the Ph.D. degree in atmospheric physics, in 1997, both from Peking University, Beijing, China.

He worked as a short-term Visiting Scholar at INRA, Paris, France, in 1998, Boston University, Boston, MA, USA, in 1999, University of Maryland, College Park, MD, USA, in 2004, and George Mason University, Fairfax, VA, USA, in 2010. He had been with the Institute of Remote Sensing Applications, Chinese Academy of Sciences, Beijing, China, from 1997 to 2012. He is currently a Professor and Deputy Director of the State Key Laboratory of Remote Sensing Science, Institute of Remote Sensing and Digital Earth, Chinese Academy of Sciences. His research interests include radiation transfer modeling for optical remote sensing and terrestrial parameter inversion from multisource remote sensing data.

He is a member of the American Geophysical Union (AGU) and the IEEE Geoscience and Remote Sensing Society(IEEE GRSS).

Longhui Li received the B.S. degree from Shenyang Agricultural University, Shenyang, China, in 2001, the M.S. degree from Nanjing Institute of Meteorology, Nanjing, China, in 2004, and the Ph.D. degree from Chinese Academy of Sciences, Beijing, China, in 2008.

Since 2012, he has been with the Plant Functional Biology and Climate Change Cluster (C3), University of Technology, Sydney, Australia, where he is currently an Australia Research Council Discovery Early Career Research Award (ARC DECRA) Research Fellow. His research interests include global terrestrial ecosystems and climate change.

Baodong Xu received the B.S. degree from Huazhong Agricultural University, Wuhan, China, in 2012. He is currently pursuing the Ph.D. degree at the University of Chinese Academy of Sciences, Beijing, China.

His research interests include validation and uncertainty analysis of remotely sensed LAI product and LAI inversion.

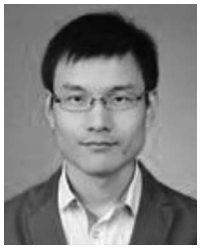

Gaofei Yin received the M.S. degree from Nanjing University, Nanjing, China, in 2012. He is currently pursing the Ph.D. degree at the University of Chinese Academy of Sciences, Beijing, China.

His research interests include radiative transfer modeling and LAI inversion.

Jingjing Peng received the B.S. degree in remote sensing from Wuhan University, Wuhan, China, in 2009. She is currently pursing the Ph.D. degree at the University of Chinese Academy of Sciences, Beijing, China.

Her research interests include validation and uncertainty analysis of remotely sensed albedo and vegetation index products.